Natural Resources Canada
Ressources naturelles Canada

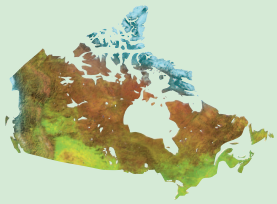

Porosity characteristics of shale samples for varied compaction zones in the Beaufort-Mackenzie Basin, Northwest Territories

T.J. Katsube, D. Issler, and S. Connell-Madore

Geological Survey of Canada

Current Research 2011-12

2011

Canada

Geological Survey of Canada
Current Research 2011-12

Porosity characteristics of shale samples for varied compaction zones in the Beaufort-Mackenzie Basin, Northwest Territories

T.J. Katsube, D. Issler, and S. Connell-Madore

2011

©Her Majesty the Queen in Right of Canada 2011

ISSN 1701-4387
Catalogue No. M44-2011/12E-PDF
ISBN 978-1-100-19136-2
doi: 10.4095/289040

A copy of this publication is also available for reference in depository libraries across Canada through access to the Depository Services Program's Web site at http://dsp-psd.pwgsc.gc.ca

A free digital download of this publication is available from GeoPub: http://geopub.nrcan.gc.ca/index_e.php

Toll-free (Canada and U.S.A.): 1-888-252-4301

Recommended citation

Katsube, T.J., Issler, D., and Connell-Madore, S., 2011. Porosity characteristics of shale samples for varied compaction zones in the Beaufort-Mackenzie Basin, Northwest Territories; Geological Survey of Canada, Current Research 2011-12, 10 p. doi: 10.4095/289040

Critical review
B. Medioli

Authors
T.J. Katsube
(John.Katsube@NRCan-RNCan.gc.ca)
S. Connell-Madore
(Shauna.Connell-Madore@NRCan-RNCan.gc.ca)
Geological Survey of Canada
601 Booth Street
Ottawa, Ontario K1A 0E8

D. Issler (Dale.Issler@NRCan-RNCan.gc.ca)
Geological Survey of Canada
3303–33 NW
Calgary, Alberta T2L 2A7

Correction date:

All requests for permission to reproduce this work, in whole or in part, for purposes of commercial use, resale, or redistribution shall be addressed to: Earth Sciences Sector Copyright Information Officer, Room 650, 615 Booth Street, Ottawa, Ontario K1A 0E9.
E-mail: ESSCopyright@NRCan.gc.ca

Porosity characteristics of shale samples for varied compaction zones in the Beaufort-Mackenzie Basin, Northwest Territories

T.J. Katsube, D. Issler, and S. Connell-Madore

Katsube, T.J., Issler, D., and Connell-Madore, S., 2011. Porosity characteristics of shale samples for varied compaction zones in the Beaufort-Mackenzie Basin, Northwest Territories; Geological Survey of Canada, Current Research 2011-12, 10 p. doi:10.4095/289040

Abstract: Effective (ϕ_E), storage (ϕ_S), and connecting (ϕ_C) porosity characteristics of 41 shale samples from nine petroleum exploration wells (952–4861 m depth) in the Beaufort-Mackenzie Basin, Northwest Territories, have been examined. These wells pass through both normally pressured and overpressured sequences and are located in four different shale compaction zones with varied Pliocene-Pleistocene sedimentation rates (50–1140 m/Ma). The purpose of this study was to determine if overpressure has had any permanent effect on the shale structure and if any relationships exist between these porosity characteristics and the sedimentation rates.

The results show no significant permanent effect from overpressure on the shale pore structure; however, the three porosity characteristics show interesting relationships with the compaction zone characteristics. Trendline fits of porosity versus depth data from different compaction zones show parallel relationships. The porosity values decrease with decreasing Pliocene-Pleistocene sedimentation rates.

Résumé : Nous avons examiné les caractéristiques de la porosité efficace (ϕ_E), de la porosité de stockage (ϕ_S) et de la porosité de communication (ϕ_C) de 41 échantillons de shale provenant de neuf puits d'exploration pétrolière (de 952 à 4861 m de profondeur) dans le bassin de Beaufort-Mackenzie (Territoires du Nord-Ouest). Ces puits traversent des séquences soumises à des conditions de pression normales et de surpression et sont situés dans quatre zones de compaction des shales différentes où les taux de sédimentation du Pliocène-Pléistocène varient (de 50 à 1140 m/Ma). Cette étude visait à déterminer si les conditions de surpression avaient un effet permanent sur la structure des shales et s'il y avait quelque relation que ce soit entre les caractéristiques de la porosité et les taux de sédimentation.

Nos résultats ne démontrent aucun effet permanent important des conditions de surpression sur la structure des pores dans les shales. Toutefois, les caractéristiques des trois types de porosité indiquent des liens intéressants avec les caractéristiques des zones de compaction. Les lignes de tendance de meilleur ajustement de la porosité en fonction de la profondeur pour les différentes zones de compaction révèlent des relations parallèles. Les valeurs de porosité décroissent avec une diminution des taux de sédimentation du Pliocène-Pléistocène.

INTRODUCTION

Porosity characteristics have been examined for 41 shale samples from normally pressured and overpressured formations in nine petroleum exploration wells from shale compaction zones 1 through 4 of the Beaufort-Mackenzie Basin, Northwest Territories (Fig. 1; Issler, 1992; Issler et al., 2002). These zones have distinctive shale compaction trends that are associated with variable Pliocene-Pleistocene sedimentation rates. The porosity data consists of effective (ϕ_E), storage (ϕ_S), and connecting (ϕ_C) porosities, determined by Connell-Madore and Katsube (2006) from mercury intrusion and extrusion porosimetry, using the pore-size distribution data of Katsube and Issler (1993). The purpose of this study was to determine if any relationships exist between these porosity characteristics and the observed compaction trends and whether overpressure has had any permanent effect on the pore-structure of the shale samples following their removal from in situ conditions.

With increased burial depth and compaction, shale can evolve into effective seals that form barriers to the upward migration of fluids and hydrocarbon gases, including CO_2. Therefore compacted shale can act as caprock for oil and gas accumulation and CO_2 sequestration and can contribute to the development of abnormal formation pressures (e.g. Huffman and Bowers, 2002) that can become a source of blowouts during drilling (e.g. Bowers, 1995). This is because the sealing capacity of shale increases as compaction reduces the number and size of the connecting pores (Bowers and Katsube, 2002). The connecting porosity, ϕ_C, mainly contributes to fluid migration; storage porosity, ϕ_S, mainly contributes to fluid storage; and effective porosity, ϕ_E is the sum of both porosity components. These are significant parameters for characterizing seal quality and for developing seal-quality evaluation methods. These three porosity types have different geophysical signatures, depending on pore structure and state of compaction (Bowers and Katsube,

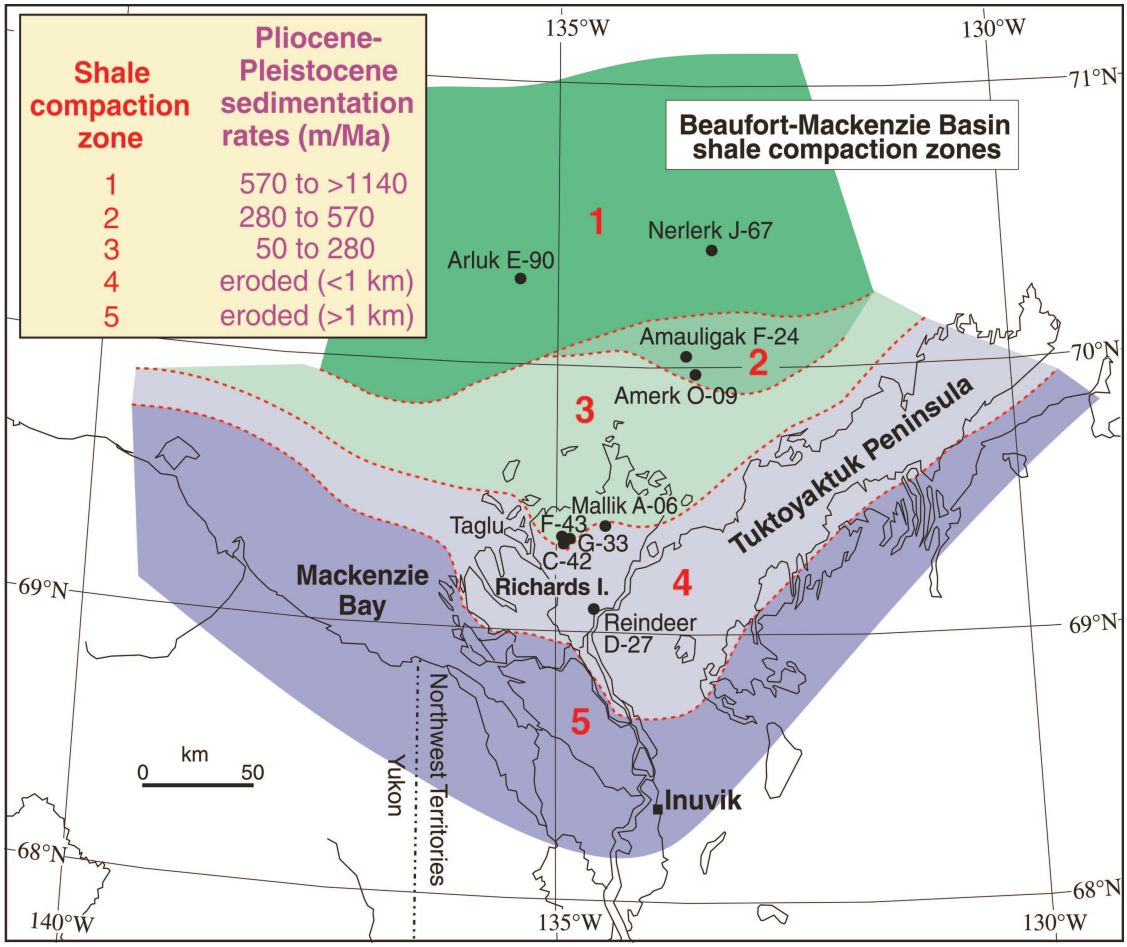

Figure 1. Location of the nine wells from which the 41 shale samples were collected in the Beaufort-Mackenzie Basin, Northwest Territories, and the approximate boundaries of the five shale compaction zones (Issler, 1992), which are shown in heavy dashed lines (Issler et al., 2002). The nine wells are numbered starting from Arluk E-90 in compaction zone 1 to Reindeer D-27 in compaction zone 4.

2002), and this can be exploited for developing advanced geophysical logging techniques for evaluating seal quality (Hermanrud et al., 1998).

SHALE COMPACTION ZONES

The 41 shale samples (Table 1) were collected from conventional cores of Cretaceous and Paleogene sediments below the Pliocene-Pleistocene formations over a depth range of approximately 950–4860 m in nine petroleum exploration wells (Katsube and Issler, 1993) in the Beaufort-Mackenzie Basin (Fig. 1). These samples are from normally pressured and overpressured sediments in four shale compaction zones (Fig. 1). The lowest compaction gradients are associated with the highest sedimentation rates (Issler, 1992). The estimated Pliocene-Pleistocene sedimentation rates for zone 1 (wells Nerlerk J-67 and Amerk E-90), zone 2 (wells Amauligak F-24 and Amerk O-09), and zone 3 (wells Taglu G-33, Taglu C-42 and Taglu F-43) are 570–1140 m/Ma, 280–570 m/Ma, and 50–280 m/Ma, respectively. The wells in zone 4 (wells Mallik A-06 and Reindeer D-27) have substantially eroded successions (Issler, 1992). Overpressure occurs below 2.3 km (main overpressure zone below 3 km) at Mallik A-06 and below approximately 2 km at Reindeer

Table 1. Sample identification (Katsube and Issler, 1993).

Well number	KB (m)	WD (m)	GL (m)	Sample ID	Depth (TVD) (m)
AMAULIGAK F-24	26.6	32.0	-	B-AM-1	3106
				B-AM-2	3119
				B-AM-3	3341
AMERK O-09	16.1	26.0	-	B-AR-1	1317
				B-AR-2	1533
				B-AR-3	1765
				B-AR-4*	3866
				B-AR-5*	4375
				B-AR-6*	4606
				B-AB-7*	4861
ARLUK E-90	12.2	58.0	-	B-AK-1*	3452
				B-AK-2*	3938
MALLIK A-06	35.5	-	27.9	B-ML-1	1362
				B-ML-2*	3176
				B-ML-3*	3547
NERLERK J-67	20.0	45.0	-	B-NR-1*	3658
				B-NR-2*	3673
				B-NR-3*	4006
REINDEER D-27	32.3	-	27.4	B-RE-1	1458
				B-RE-2	1459
				B-RE-3	2022
				B-RE-4	2092
				B-RE-5	2099
				B-RE-6*	2213
				B-RE-7*	2389
				B-RE-8*	2421
				B-RE-9*	2551
				B-RE10*	2725
				B-RE11*	2923
				B-RE-12*	3153
				B-RE-13*	3481
				B-RE-14*	3628
TAGLU C-42	12.3	-	1.7	B-TA-1	2881
TAGLU F-43	12.0	-	1.4	B-TA-2*	3247
TAGLU G-33	7.9	-	1.8	B-TG-1	952
				B-TG-2	1350
				B-TG-3	1640
				B-TG-4	2075
				B-TG-5	2459
				B-TG-6	2460
				B-TG-7	2533

KB: Kelly bushing elevation.
WD: Water depth.
GL: Ground level.
Samples marked with (*) are from overpressured formations.
TVD: True vertical depth values.

D-27 (Issler et al., 2002). Further details on the regional stratigraphy can be found in related publications (Issler, 1992; Issler et al., 2002).

Examples of shale sonic porosity, ϕ_G, determined using downhole sonic logs and the method of Issler (1992) versus depth (h) relationships, are shown in Figure 2 for four of the nine wells. Figure 2a shows the ϕ_G-h relationship for well Amerk O-09 representing the trend in zone 1 and zone 2. Figures 2b and 2c show the ϕ_G-h relationship for wells Taglu G-33 and Mallik A-06, representing the trends in zone 3 and the northern part of zone 4, respectively. Figure 2d shows the ϕ_G-h relationship for well Reindeer D-27, representing the trend in the southern section of zone 4. Figure 2 shows that compaction gradients (CG) in the normally pressured zone increase from approximately 0.9%/100 m in zone 2 to nearly 1.2%/100 m in zone 4. The CG is represented by the sonic porosity per cent decrease per 100 m depth (ϕ_G%/100 m). Although these differences are relatively small, they are consistent with the larger data set of Issler (1992) that shows an increase in CG with declining sedimentation rate from offshore to onshore regions.

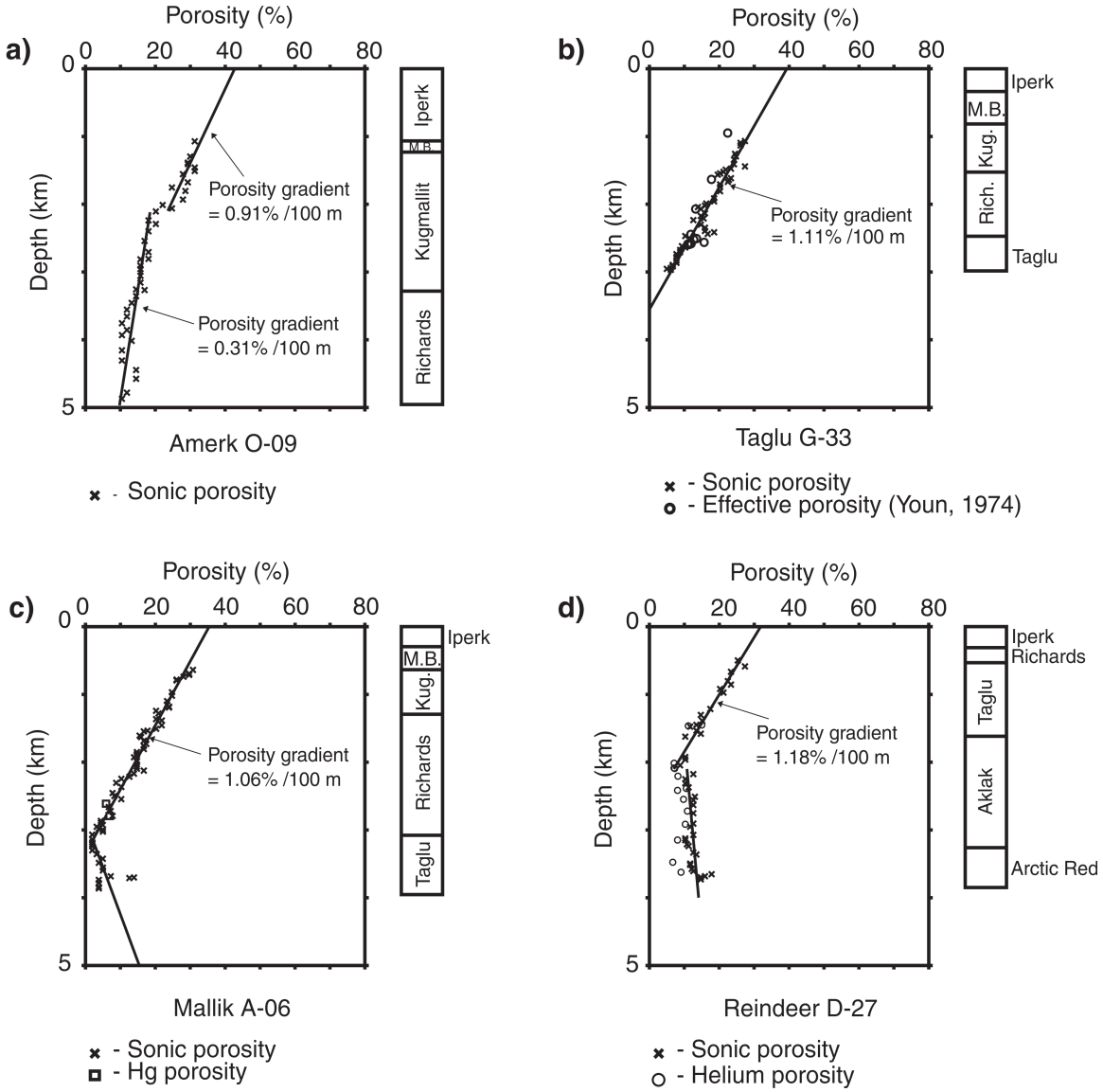

Figure 2. Examples of the sonic porosity (ϕ_G), determined by using downhole sonic logs and the method of Issler (1992) versus depth (h) relationship for four of the nine wells in the compaction zones (Fig. 1). **a)** The ϕ_G-h relationship for well Amerk O-09 (zone 2) representing the trend in compaction zones 1 and 2. **b)**, **c)** The ϕ_G-h relationship for well Taglu G-33 (compaction zone 3) and Mallik A-06 (compaction zone 4), representing the trends in the northern section of compaction zone 4 and southern section of zone 3. **d)** The ϕ_G-h relationship for well Reindeer D-27 (compaction zone 4), representing the trend in the southern section of compaction zone 4. Sequence names: M.B. = Mackenzie Bay; Kug., = Kugmallit; Rich., = Richards; Hg porosity from Katsube and Issler (1993) and helium porosity from Issler and Katsube (1994).

METHOD OF INVESTIGATION

Connell-Madore and Katsube (2006) used the ϕ_E values of Katsube and Issler (1993) and the corresponding mercury intrusion and extrusion data to determine the ϕ_S and ϕ_C values (Fig. 3) for the 41 shale samples used in this study. Details of the mercury porosimetry method and the procedures for obtaining the three porosities (ϕ_E, ϕ_S, ϕ_C) are described in Katsube (2000) and Connell-Madore and Katsube (2006). By this method mercury is forced into a shale sample under pressure, and the total volume of mercury intruded is used to determine the ϕ_E. The total amount of mercury that extrudes from the sample after the pressure is released (Fig. 3) is used to determine the ϕ_C (Wardlaw and Taylor, 1976). The ϕ_S, which represents the amount of mercury trapped in the sample after the pressure is released, is determined by the difference between ϕ_E and ϕ_C. The ϕ_S represents mainly the intergranular pore space, whereas ϕ_C represents the interconnected pore space between the storage pores (Fig. 4), and provides the main pathway for fluid migration in these shale samples. The ϕ_E is the sum of these two porosities but is not the total porosity (ϕ_T) of a rock, because it does not include the pore space of isolated pores. According to a previous study (Bowers and Katsube, 2002), ϕ_C is more sensitive to overpressure than ϕ_S in deep formations.

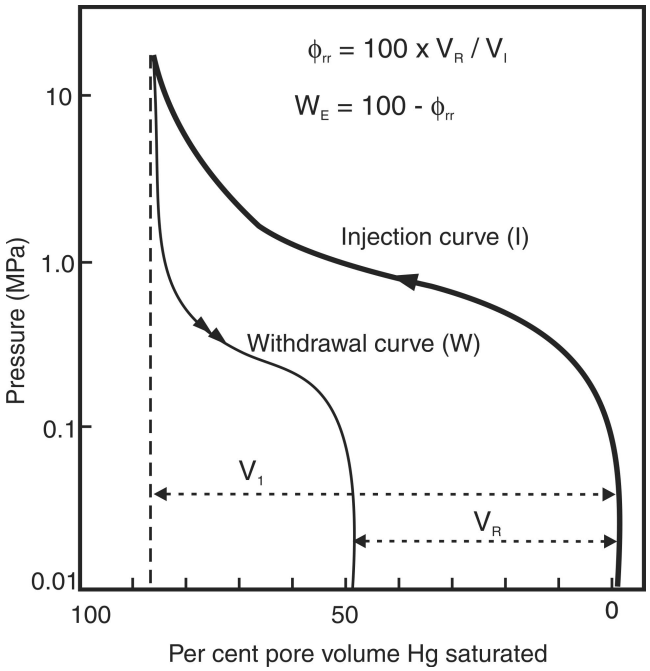

Figure 3. Diagram (*modified from* Wardlaw and Taylor, 1976) describing the mercury intrusion and extrusion curves and explaining the definitions and methods for determining withdrawal efficiency (W_E) and storage porosity ratio ($\phi_{rr} = \phi_S/\phi_E$). The V_I and V_R are the total mercury intrusion volume and total residual volume, respectively. The intrusion and extrusion curves are represented by injection curve (I) and withdrawal curve (W) in this diagram.

In this study, the 41 shale samples are grouped into three study zones, SZ-12, SZ-4N, and SZ-4S, in order of lower to higher compaction gradient (CG = ϕ_G%/100 m). There are only five samples from compaction zone 1 and they are from near the bottom of wells Arluk E-90 and Nerlerk J-67 (Fig. 1, Table 1). Therefore, they were lumped together with the ten samples from compaction zone 2 that cover a broader depth range (wells Amauligak F-24 and Amerk O-09) to form SZ-12. Study zone SZ-4N consists of 12 samples from four wells (Mallik A-06, Taglu F-43, Taglu G-33, and Taglu C-42) close to the boundary between compaction zones 3 and 4 (Fig. 1, Table 1). Fourteen samples from the Reindeer D-27 well in the southern part of compaction zone 4 are included in SZ-4S (Fig. 1, Table 1).

EXPERIMENTAL RESULTS

The experimental results of the three porosities (ϕ_E, ϕ_S, ϕ_C) and the ϕ_C/ϕ_E ratio values for the 41 samples from the nine wells (Fig. 1) are listed in Tables 2 and 3. The four compaction zones with the different Pliocene-Pleistocene sedimentation rates for which the wells are located are also listed in these tables.

The porosity versus depth relationships for the three porosities (ϕ_E, ϕ_S, ϕ_C) and the ϕ_C/ϕ_E ratio values in all nine wells are shown in Figure 5. The same plots are also broken down by study zones in Figure 6 (SZ-12), Figure 7 (SZ-4N), and Figure 8 (SZ-4S).

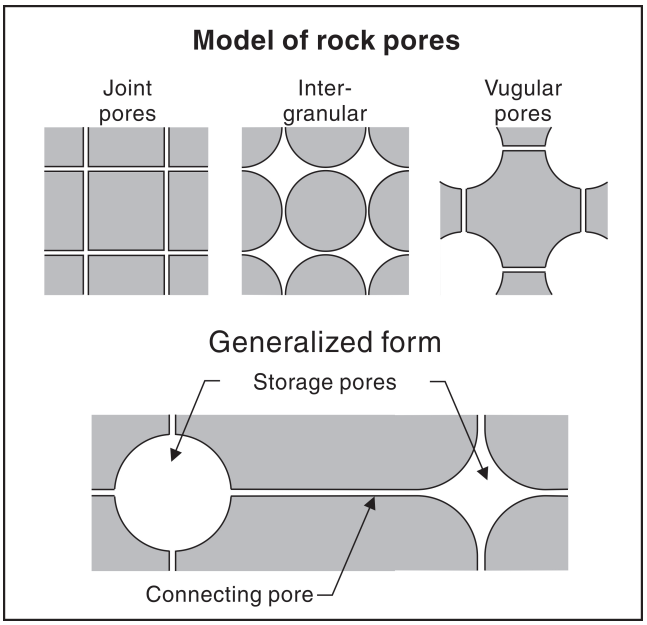

Figure 4. Storage and connecting pore model used for characterizing shale samples (Katsube and Williamson, 1994, 1998). The ϕ_S represents the storage porosity, and ϕ_C represents the connecting porosity which provides the pathway for fluid migration in these shale samples.

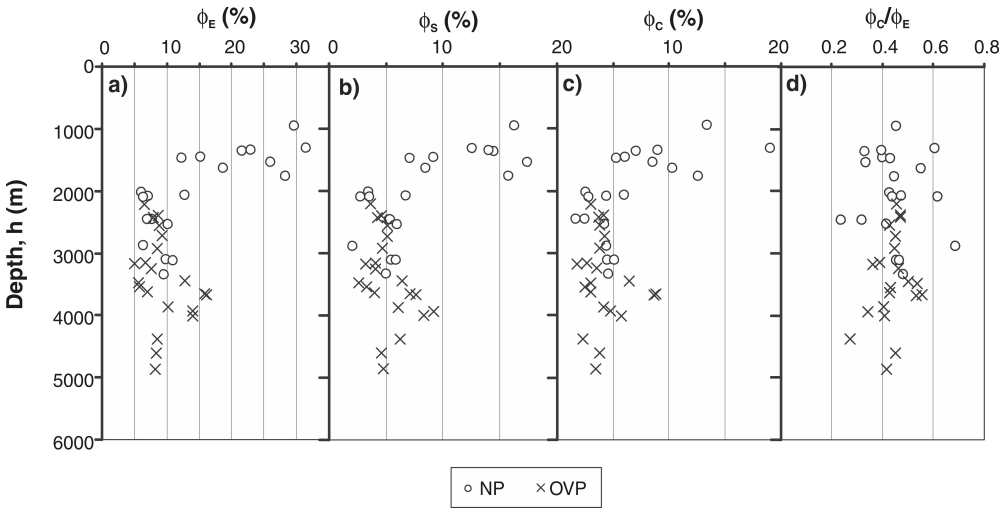

Figure 5. Porosity versus depth (h) relationships for the three porosity (ϕ_E, ϕ_S, ϕ_C) types and the ϕ_C /ϕ_E ratio versus depth in all nine wells; **a**) ϕ_E versus depth for all nine wells, **b)** ϕ_S versus depth for all nine wells, **c)** ϕ_C versus depth (h) for all nine wells; and **d)** ϕ_C /ϕ_E versus depth for all nine wells. (NP = normally pressured, OVP = over pressured).

Table 2. Porosity data for 17 out of the 41 shale samples used in this study, which are all from compaction zone 4. Samples marked with an asterisk are from over-pressured areas. All other samples are from normally-pressured areas.

Sample number	TVD (m)	ϕ_E (%)	ϕ_S (%)	ϕ_C (%)	ϕ_C/ϕ_E
B-ML-1	1362	21.4	14.4	7	0.33
B-ML-2*	3176	5	3.2	1.8	0.36
B-ML-3*	3547	5.8	3.3	2.5	0.43
B-RE-1	1458	15.1	9.1	6	0.4
B-RE-2	1469	12.2	7	5.2	0.43
B-RE-3	2022	5.9	3.4	2.5	0.42
B-RE-4	2092	7	2.7	4.3	0.61
B-RE-5	2099	6.2	3.5	2.7	0.44
B-RE-6*	2213	6.6	3.6	3	0.46
B-RE-7*	2389	8.7	4.6	4.1	0.47
B-RE-8*	2421	7.9	4.2	3.7	0.47
B-RE-9*	2551	8.9	5.1	3.8	0.43
B-RE-10*	2725	9.3	5.1	4.2	0.45
B-RE-11*	2923	8.5	4.7	3.8	0.45
B-RE-12*	3153	6.7	4.1	2.6	0.39
B-RE-13*	3481	5.6	2.6	3	0.54
B-RE-14*	3628	7	4	3	0.43

TVD: True vertical depth values.
ϕ_E: Effective porosity.
ϕ_S: Storage porosity.
ϕ_C: Connecting porosity.

Table 3. Porosity data for 24 out of the 41 shale samples used in this study, from compaction zones 1 through 3. Samples marked with an asterisk are from over-pressured areas. All other samples are from normally-pressured areas.

Sample number	TVD (m)	ϕ_E (%)	ϕ_S (%)	ϕ_C (%)	ϕ_C/ϕ_E	Compaction zone
B-TG-1	952	29.5	16.2	13.3	0.45	3
B-TG-2	1350	22.8	13.9	8.9	0.39	3
B-TG-3	1640	18.6	8.4	10.2	0.55	3
T-BG-4	2075	12.6	6.7	5.9	0.47	3
B-TG-5	2459	7.6	5.2	2.4	0.32	3
B-TG-6	2460	6.9	5.3	1.6	0.23	3
B-TG-7	2533	10	5.9	4.1	0.41	3
B-TA-1	2881	6.3	2	4.3	0.68	3
B-TA-2*	3247	7.6	4.1	3.5	0.46	3
B-AM-1	3106	9.8	5.4	4.4	0.44	2
B-AM-2	3119	10.8	5.8	5	0.46	2
B-AM-3	3341	9.4	4.9	4.5	0.48	2
B-AR-1	1317	31.4	12.5	18.9	0.6	2
B-AR-2	1533	25.8	17.3	8.5	0.33	2
B-AR-3	1765	28.2	15.7	12.5	0.44	2
B-AR-4*	3866	10.2	6.1	4.1	0.4	2
B-AR-5*	4375	8.5	6.2	2.3	0.27	2
B-AR-6*	4606	8.4	4.6	3.8	0.45	2
B-AR-7*	4861	8.2	4.8	3.4	0.42	2
B-NR-1*	3658	15.9	7.1	8.8	0.55	1
B-NR-2*	3673	16.2	7.6	8.6	0.53	1
B-NR-3*	4006	14	8.3	5.7	0.41	1
B-AK-1*	3452	12.8	6.4	6.4	0.5	1
B-AK-2*	3938	14	9.2	4.8	0.34	1

TVD: True vertical depth values.
ϕ_E: Effective porosity.
ϕ_S: Storage porosity.
ϕ_C: Connecting porosity.

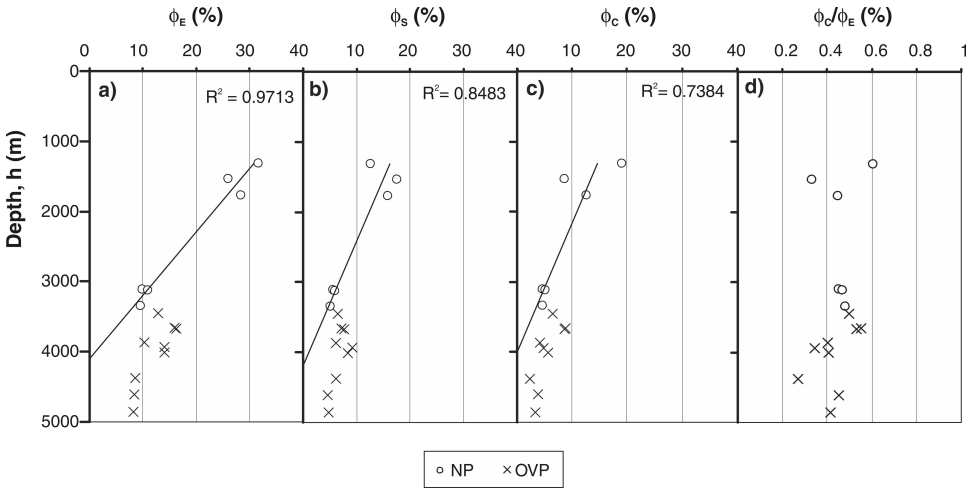

Figure 6. Porosity versus depth (h) relationships for the three porosities (ϕ_E, ϕ_S, ϕ_C) and the ϕ_C/ϕ_E ratio versus depth values for the four wells in study zone SZ-12 (wells Arluk E-90, Nerlerk J-67, Amaulligak F-24, and Amerk O-09); **a)** ϕ_E versus depth for all four wells, **b)** ϕ_S versus depth for all four wells, **c)** ϕ_C versus depth for all four wells, and **d)** ϕ_C /ϕ_E versus depth for all four wells. (NP = normally pressured, OVP = over pressured, R^2 = R squared for the trendline.

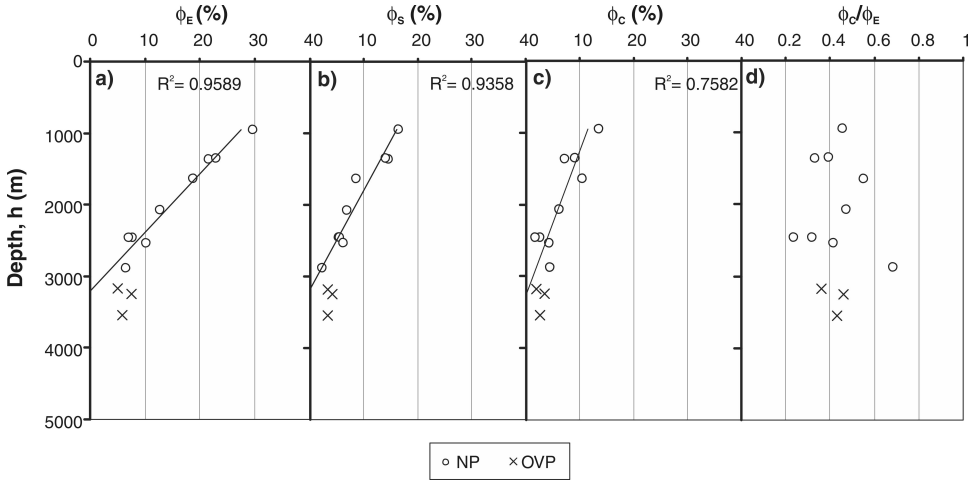

Figure 7. Porosity versus depth (h) relationships for the three porosities (ϕ_E, ϕ_S, ϕ_C) and the ϕ_C/ϕ_E ratio versus h values for the four wells (wells Taglu C-42, Taglu F-43, Taglu G-33, Mallik A-06) in study zone SZ-4N; **a)** ϕ_E versus depth for all four wells, **b)** ϕ_S versus depth for all four wells, **c)** ϕ_C versus depth for all four wells, and **d)** ϕ_C /ϕ_E versus depth for all four wells. (NP = normally pressured, OVP = over pressured, R^2 = R squared for the trendline.

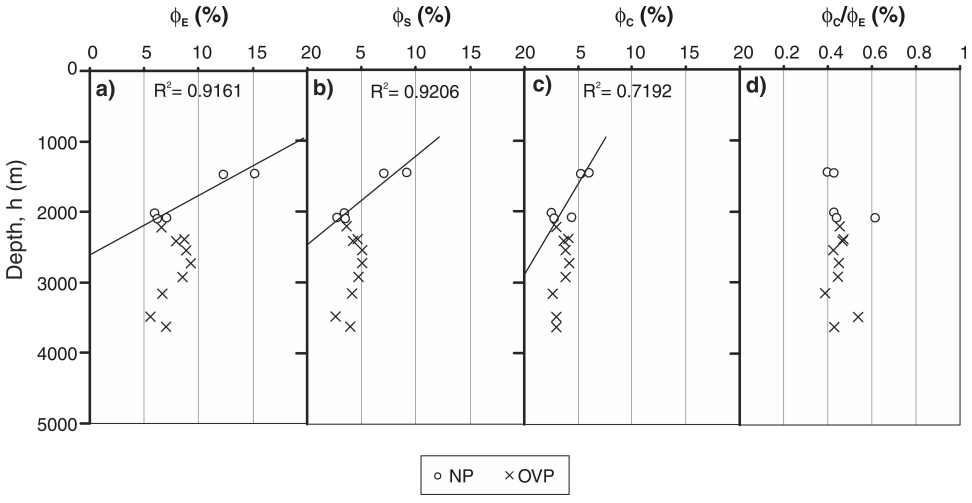

Figure 8. Porosity versus depth (h) relationships for the three porosities (ϕ_E, ϕ_S, ϕ_C) and the ϕ_C/ϕ_E versus h values in well Reindeer D-27 representing study zone SZ-4S; **a)** ϕ_E versus depth, **b)** ϕ_S versus depth, **c)** ϕ_C versus depth, **d)** ϕ_C / ϕ_E versus depth. (NP = normally pressured, OVP = over pressured, R^2 = R squared for the trendline.

Table 4. Curve-fitted coefficients for study zones SZ-12, SZ-4N, and SZ-4S, and the curve-fitted maximum porosity and curve-fitted depth of maximum compaction for the trendlines of **a)** ϕ_E/h, **b)** ϕ_S/h, and **c)** ϕ_C/h.

a) ϕ_E/h trendlines

Compaction study zones	SZ-12	SZ-4N	SZ-4S
ϕ_{EX} (%)	45.3	39.15	30.95
k_{EX} (%/100 m)	1.10	1.22	1.19
h_{EMX} (m)	4117.7	3208.9	2600.8
R^2	0.97	0.96	0.92

ϕ_{EX} = Curve-fitted maximum effective porosity (Equation 1).
k_{EX} = Porosity versus depth gradient per 100 m depth.
h_{EMX} (m) = Curve-fitted depth of maximum compaction.
R^2 = R-squared.

b) ϕ_S/h trendlines

Compaction study zones	SZ-12	SZ-4N	SZ-4S
ϕ_{SX} (%)	23.5	22.85	19.71
k_{SX} (%/100 m)	0.56	0.72	0.80
h_{SMX} (m)	4199.6	3174.2	2463.8
R^2	0.85	0.94	0.92

ϕ_{SX} = Curve-fitted coefficient for maximum storage porosity
k_{SX} = Porosity versus depth gradient per 100 m depth.
h_{MX} (m) = Curve-fitted depth of maximum compaction.

c) ϕ_C/h trendlines

Compaction study zones	SZ-12	SZ-4N	SZ-4S
ϕ_{CX} (%)	21.8	16.3	11.24
k_{CX} (%/100 m)	0.54	0.50	0.39
h_{CMX} (m)	4032.8	3259	2882.1
R^2	0.74	0.76	0.72

ϕ_{CX} = Curve-fitted coefficient for maximum connecting porosity.
k_{CX} = Porosity versus depth gradient per 100 m depth.
h_{CMX} (m) = Curve-fitted depth of maximum compaction.

DATA ANALYSIS

All three porosities (ϕ_E, ϕ_S, ϕ_C), when grouped together for the three study zones (SZ) as displayed in Figure 5, show a rather rapid decrease with increased depth until about 2000–3000 m. This depth is considered the depth of maximum compaction (h_{MX}) in this study. Beyond that depth, there is a slight rise in some of the porosity values until a depth of about 3500–5000 m, mostly for the samples from the overpressured formations. The depth range from the surface to the maximum depth of compaction (h_{MX}) is considered to be, in this study, the initial stage of compaction. The rate of porosity decrease with depth for the initial stage of compaction is not necessarily identical for the different study zones, as shown in Figures 6, 7, and 8.

The ϕ_E versus depth (h) gradient (ϕ_E/h) relationships of the initial stages of compaction for study zones SZ-12, SZ-4N, and SZ-4S are shown in Figures 6a, 7a, and 8a, respectively. The initial stages of these ϕ_E/h relationships, in all three figures, are generally linear with a rather steep ϕ_E/h until h_{MX}. The trendline function of Excel was used to fit the data in Figures 6a, 7a, and 8a. That Excel trendline function has been simulated by the following general linear function, by using the parameters, ϕ_E, k_E, h, ϕ_{EX}, used in this study:

$$\phi_E = -k_E h + \phi_{EX}, \qquad (1)$$

where k_E is the effective porosity versus depth gradient (ϕ_E/h) and ϕ_{EX} is the curve fitted effective porosity at h = 0. The k_E, ϕ_{EX} and R^2 values for the data are all listed in Table 4. The R^2 values for the trendlines in Figures 6a, 7a, and 8a are 0.97, 0.96, and 0.92 (Table 4), respectively, indicating a small scatter of the ϕ_E values, and can be considered to represent very good fits. When ϕ_E is equal to zero in Equation 1, a depth expressed by h_{EMX} can be determined by the following equation:

$$h_{EMX} = \phi_E / k_E. \qquad (2)$$

This h_{EMX} is referred to as the curve fitted maximum-compaction depth in this study. The h_{EMX} values for Figures 6a, 7a, and 8a are also listed in Table 4. The trendlines for the initial stages of the ϕ_S versus depth and ϕ_C versus depth have

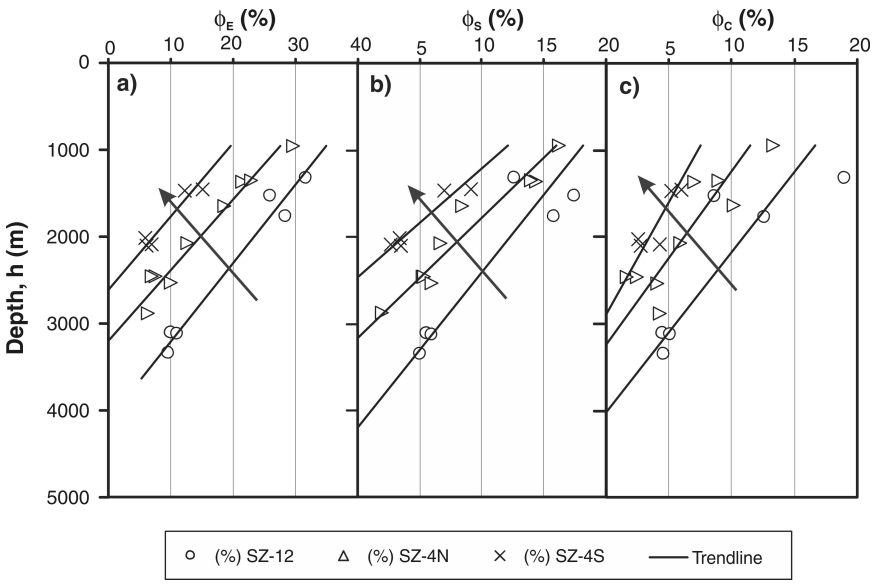

Figure 9. Comparison of the trendlines for the initial stages (900–3000 m depth ranges) of the three porosities from the three study zones (SZ-12, SZ-4N, and SZ-4S), for **a)** ϕ_E versus depth, **b)** ϕ_S versus depth, and **c)** ϕ_C versus depth. The arrow shows the direction toward the zone of higher compaction.

also been determined and entered into Figures 6b, 6c, 7b, 7c, 8b, and 8c, using the same procedure as for ϕ_E versus depth. The R^2 values for the ϕ_S versus depth data are in the range of 0.85 to 0.94 as shown in the corresponding figures. The same values for the ϕ_C versus depth values are in the range of 0.72 to 0.76, indicating a considerably larger scatter than the other two porosities. In Figure 9, the trendlines for the initial stages of each porosity type versus depth for each of the study zones are displayed. The curve fitted storage and connecting porosities determined by these trendlines for the ϕ_S and ϕ_C data sets are expressed by ϕ_{SX} and ϕ_{CX}, and the curve fitted maximum compaction depths for the same trendlines are expressed by h_{SMX} and h_{CMX} (Table 4).

Details of the trendline characteristics are listed in Table 4. In this table the effective porosity versus depth gradient is expressed by the porosity decrease per 100 m depth and represented by k_{EX} (ϕ_E%/100 m) rather than k_E, which is the case in Equations 1 and 2. The reason for this change in expression is to enable a comparison between the effective porosity versus depth gradients and the compaction gradient (ϕ_G%/100 m) values.

DISCUSSION AND CONCLUSIONS

Bowers and Katsube (2002) showed that ϕ_C increases significantly more than ϕ_S in highly compacted shale rocks in response to overpressure, implying that ϕ_C is more sensitive to overpressure than ϕ_S. Since ϕ_E is the sum of ϕ_C and ϕ_S, this implies that the values of the ϕ_C/ϕ_E ratio for the samples from overpressured formations should be larger than those from the normally pressured formations; however, in this study it appears that no difference can be identified between the ϕ_C/ϕ_E values of the shale samples from the normally pressured and overpressured formations. For example, the ϕ_C/ϕ_E values in Figure 8d are almost constant over both overpressured and normally pressured formations. In Figures 6d and 7d the ϕ_C/ϕ_E values are more scattered, but there is no obvious difference in the trend between the samples from the normally pressured and overpressured formations. This is confirmed by comparing average ϕ_C/ϕ_E values (± one standard deviation) corresponding to study zones SZ-12, SZ-4N, and SZ-4S for normally pressured (0.46 ± 0.09, 0.43 ± 0.13, and 0.46 ± 0.09) and overpressured (0.43 ± 0.09, 0.42 ± 0.05, and 0.45 ± 0.04) formations.

The reason for the difference between the laboratory results of Bowers and Katsube (2002) and those of this study is likely because the former measurements were made under overpressured conditions whereas the latter were conducted under surface pressure conditions. This suggests that high laboratory fluid pressure for the porosity measurements may have increased the ϕ_C values for the Bowers and Katsube (2002) study. In conclusion, it appears that the geological in situ overpressure has not permanently affected the shale pore structure by increasing the ϕ_C/ϕ_E ratio.

The downhole sonic porosity versus depth gradient (CG = ϕ_G%/100 m) values for study zones SZ-12, SZ-4N, and SZ-4S (Fig. 2) are 0.91, 1.06, and 1.18, respectively, showing that porosity gradient increases from offshore regions to more consolidated onshore regions to the south. The effective porosity versus depth gradient (K_{EX} = ϕ_E%/100 m) (Table 4) values for the same study zones are 1.10, 1.22, and 1.19, respectively. There are fewer data points to constrain the K_{EX}

trends so it is not surprising that they differ somewhat from the trend of CG values; however they do indicate a general increase in porosity gradient from offshore to onshore areas.

The ϕ_E/h trendlines for the three study zones in Figure 9a show an interesting trend. They are generally parallel and both their curve-fitted maximum effective porosities and curve-fitted maximum depth of compaction values decrease southward toward areas of increased compaction. This pattern likely results from exhumation of strata along the southern basin margin (Issler, 1992). The trendlines of the initial stages of the ϕ_S/h and ϕ_C/h for the three study zones displayed in Figures 9b and 9c also show similar trends, although they are not as parallel as those of the ϕ_E/h trendlines. This may be related to the basin stress history (Issler, 1992). Sediments in zone SZ-12 are overlain by a thick Pliocene-Pleistocene succession and are presently at their maximum burial depth. The ϕ_S and ϕ_C show a similar variation with depth in zone 12. In contrast, onshore areas have experienced variable erosion and show larger differences between ϕ_S and ϕ_C. For example, zone SZ-4S has experienced the most erosion (Issler, 1992) and largest decrease in overburden stress. The ϕ_S shows a greater change with depth than ϕ_C in this area (Figure 9b, c; Table 4).

ACKNOWLEDGMENTS

The authors express their gratitude to B. Medioli (GSC Ottawa) for critically reviewing this paper and for her very constructive and interesting suggestions. The authors express their gratitude to F.P. Agterberg (GSC Ottawa) for his advice on the curve-fitting methods. The authors express their gratitude to E. Inglis (Scientific and Technical Publishing Services/Mapping Information Branch) for her suggested changes and additions for this paper.

REFERENCES

Bowers, G.L., 1995. Pore pressure estimation from velocity data: accounting for overpressure mechanisms besides undercompaction; Society of Petroleum Engineers Drilling and Completion, June, p. 89–95.

Bowers, G.L. and Katsube, T.J., 2002. The role of shale pore-structure on the sensitivity of wireline logs to overpressure; *in* Pressure regimes in sedimentary basins and their prediction, (ed.) A.R. Huffman and G.L. Bowers; American Association of Petroleum Geologists Memoir 76, p. 43–60.

Connell-Madore, S. and Katsube, T.J., 2006. Pore-size distribution characteristics of Beaufort-Mackenzie Basin shale samples, Northwest Territories; *in* Geological Survey of Canada, Current Research 2006-B1, 13 p. doi:10.4095/222398

Hermanrud, C., Wensaas, L., Teige, G.M.G., Vike, E., Nordgrd Bols, H.M., and Hansen, S., 1998. Shale porosities from well logs on Haltenbanken (offshore mid-Norway) show no influence of overpressuring; *in* Abnormal pressures in hydrocarbon environments, (ed.) B.E. Law, G.F. Ulmishek, and V.I. Slavin; American Association of Petroleum Geologists, Memoir 70, p. 65–85.

Huffman, .R. and Bowers, G.L. (ed.), 2002. Pressure Regimes in Sedimentary Basins and their Prediction; American Association of Petroleum Geologists, Memoir 76, 238 p.

Issler, D.R., 1992. A new approach to shale compaction and stratigraphic restoration, Beaufort-Mackenzie Basin and Mackenzie Corridor, northern Canada; The American Association of Petroleum Geologists Bulletin, v. 76, p. 1170–1189.

Issler, D.R. and Katsube, T.J., 1994. Effective porosity of shale samples from the Beaufort-Mackenzie Basin, northern Canada; *in* Current Research, Part B; Geological Survey of Canada, Paper 94-1B, p. 19–26.

Issler, D.R., Katsube, T.J., Bloch, J.D., and McNeil, D.H., 2002. Shale compaction and overpressure in the Beaufort-Mackenzie Basin of northern Canada; Geological Survey of Canada, Open File 4192, 10 p. (CD-ROM). doi:10.4095/213052

Katsube, T.J., 2000. Shale permeability and pore-structure evolution characteristics; implications for overpressure; *in* Geological Survey of Canada, Current Research 2000-E15, 9 p. doi:10.4095/211622

Katsube, T.J. and Issler, D.R., 1993. Pore-size distributions of shales from the Beaufort-Mackenzie Basin, northern Canada; *in* Geological Survey of Canada, Current Research 93-1E, p. 123–132.

Katsube, T.J. and Williamson, M.A., 1994. Shale petrophysics and basin charge modelling; *in* Current Research, Part D; Geological Survey of Canada, Paper 94-1D, p. 179–188.

Katsube, T.J. and Williamson, M.A., 1998. Shale petrophysical characteristics: permeability history of subsiding shales; *in* Shales and mudstones II, (ed.) J. Schieber, W. Zimmerle, and P.S. Sethi; Stuttgart, Germany, p. 69–91.

Wardlaw, N.C. and Taylor, R.P., 1976. Mercury capillary pressure curves and the interpretation of pore structure and capillary behaviour in reservoir rocks; Bulletin of Canadian Petroleum Geology, v. 24, p. 225–262.

Geological Survey of Canada Project EGM003